



OPEN ACCESS

EDITED BY

Evren Özarlan,
Linköping University, Sweden

REVIEWED BY

Adil Bashir,
Auburn University, United States
Andrew L. Alexander,
University of Wisconsin-Madison,
United States

*CORRESPONDENCE

Madhura Baxi
mbaxi@bu.edu

†These authors have contributed
equally to this work

SPECIALTY SECTION

This article was submitted to
Brain Imaging Methods,
a section of the journal
Frontiers in Neuroimaging

RECEIVED 18 May 2022

ACCEPTED 19 July 2022

PUBLISHED 13 September 2022

CITATION

Baxi M, Cetin-Karayumak S,
Papadimitriou G, Makris N, van der
Kouwe A, Jenkins B, Moore TL,
Rosene DL, Kubicki M and Rathi Y
(2022) Investigating the contribution of
cytoarchitecture to diffusion MRI
measures in gray matter using
histology.
Front. Neuroimaging 1:947526.
doi: 10.3389/fnimg.2022.947526

COPYRIGHT

© 2022 Baxi, Cetin-Karayumak,
Papadimitriou, Makris, van der Kouwe,
Jenkins, Moore, Rosene, Kubicki and
Rathi. This is an open-access article
distributed under the terms of the
[Creative Commons Attribution License
\(CC BY\)](#). The use, distribution or
reproduction in other forums is
permitted, provided the original
author(s) and the copyright owner(s)
are credited and that the original
publication in this journal is cited, in
accordance with accepted academic
practice. No use, distribution or
reproduction is permitted which does
not comply with these terms.

Investigating the contribution of cytoarchitecture to diffusion MRI measures in gray matter using histology

Madhura Baxi^{1,2*}, Suheyla Cetin-Karayumak²,
George Papadimitriou³, Nikos Makris², Andre van der Kouwe⁴,
Bruce Jenkins⁴, Tara L. Moore^{5,6}, Douglas L. Rosene^{5,6},
Marek Kubicki^{2,4†} and Yogesh Rathi^{2,4†}

¹Graduate Program for Neuroscience, Boston University, Boston, MA, United States, ²Psychiatry Neuroimaging Laboratory, Brigham and Women's Hospital, Harvard Medical School, Boston, MA, United States, ³Center for Morphometric Analysis, Massachusetts General Hospital, Charlestown, MA, United States, ⁴Martinos Center for Biomedical Imaging, Massachusetts General Hospital, Charlestown, MA, United States, ⁵Anatomy and Neurobiology, Boston University School of Medicine, Boston, MA, United States, ⁶Center for Systems Neuroscience, Boston, MA, United States

Postmortem studies are currently considered a gold standard for investigating brain structure at the cellular level. To investigate cellular changes in the context of human development, aging, or disease treatment, non-invasive *in-vivo* imaging methods such as diffusion MRI (dMRI) are needed. However, dMRI measures are only indirect measures and require validation in gray matter (GM) in the context of their sensitivity to the underlying cytoarchitecture, which has been lacking. Therefore, in this study we conducted direct comparisons between *in-vivo* dMRI measures and histology acquired from the same four rhesus monkeys. Average and heterogeneity of fractional anisotropy and trace from diffusion tensor imaging and mean squared displacement (MSD) and return-to-origin-probability from biexponential model were calculated in nine cytoarchitecturally different GM regions using dMRI data. DMRI measures were compared with corresponding histology measures of regional average and heterogeneity in cell area density. Results show that both average and heterogeneity in trace and MSD measures are sensitive to the underlying cytoarchitecture (cell area density) and capture different aspects of cell composition and organization. Trace and MSD thus would prove valuable as non-invasive imaging biomarkers in future studies investigating GM cytoarchitectural changes related to development and aging as well as abnormal cellular pathologies in clinical studies.

KEYWORDS

diffusion MRI, histology, validation, gray matter, rhesus monkey, imaging biomarkers

Introduction

Diffusion MRI is a widely used *in-vivo* imaging method that measures the displacement of water molecules within brain tissue. Since the water movement is affected directly by the underlying biology, dMRI can provide a non-invasive measure of the underlying tissue microstructure and offers a unique opportunity to conduct

neuroimaging studies investigating microstructural brain changes. DMRI has been shown to be sensitive to changes in gray and white matter associated with brain development (Tanner et al., 1999; Yoshida et al., 2013), and aging (Giorgio et al., 2010; Lebel et al., 2012), as well as psychiatric and neurological disorders such as amyotrophic lateral sclerosis (ALS) (Baek et al., 2020), multiple sclerosis (MS) (Inglese and Bester, 2010), traumatic brain injury (TBI) (Laitinen et al., 2015; Zhang et al., 2017), Alzheimer's disease (Stebbins and Murphy, 2009), Parkinson's disease (Zhang and Burock, 2020), depression (Coloigner et al., 2019), and schizophrenia (Kubicki et al., 2007). Characterization of brain microstructure with this imaging method thus provides an opportunity to study developmental and aging related changes as well as disease related abnormalities.

However, dMRI can only provide indirect measures of the underlying microstructural properties of the tissue due to limited spatial resolution of the data. Further, dMRI provides an ensemble average of the displacement of water molecules within cell bodies, its processes (axons, dendrites), and extra-cellular spaces which are several orders of magnitude smaller than the millimeter scale image resolution. This necessitates the need for validation of dMRI measures. Currently, postmortem histological studies remain the gold standard to study tissue microstructure. So far, they have provided important information about gray matter (GM) microstructure at the cellular level, in healthy individuals as well as patients with psychiatric and neurological disorders (Huttenlocher, 1979, 1984; Rakic et al., 1986; Stockmeier and Rajkowska, 2004; Williams et al., 2013; Khaw et al., 2021). Therefore, validating the biological basis of these dMRI measures using postmortem tissue from animals scanned pre-mortem can help establish the specificity and the interpretation of diffusion MRI studies in healthy and clinical populations as well as push the frontiers for the diagnosis and treatment of neurological and psychiatric disorders.

Several studies have been conducted in white matter for *ex-vivo* validation of dMRI models and the derived measures against relevant histological measures. These studies include those that validate dMRI tractography, fiber orientation, and other microstructural properties of axonal bundles estimated using various dMRI models, e.g., diffusion tensor imaging (DTI), high angular resolution diffusion-weighted imaging (HARDI), neurite orientation dispersion and density imaging (NODDI), and white matter tract integrity (WMTI) (Leergaard et al., 2010; Gao et al., 2013; Schilling et al., 2018; Gutierrez et al., 2020; Zhou et al., 2020; Leuze et al., 2021; Yendiki et al., 2021) with the relevant histological measures. Histological measures were computed in these dMRI validation studies, using various postmortem techniques such as neural tracer data (Gutierrez et al., 2020), myelin stains (Zhou et al., 2020), label-free optical imaging techniques (Yendiki et al., 2021), and optical imaging of fluorescently labeled neurofilaments and vasculature

in 3D tissue cuboids cleared using the clear lipid-exchanged acrylamide-hybridized rigid imaging/immunostaining/*in situ*-hybridization-compatible tissue hydrogel (CLARITY) (Leuze et al., 2021). Animal models such as rats (Leergaard et al., 2010), marmosets (Gutierrez et al., 2020), squirrel monkeys (Schilling et al., 2018), macaques (Leuze et al., 2021) and humans (Zhou et al., 2020) were used to conduct these studies.

All of the above studies were primarily focused on white matter microstructure validation. In contrast, only a handful of studies have conducted postmortem validation of dMRI models and derived measures in GM (Kroenke et al., 2007; Bock et al., 2010; Jespersen et al., 2012; Laitinen et al., 2015; Seehaus et al., 2015; Khan et al., 2016; Dyrby et al., 2018; Shimony et al., 2018; Maiter et al., 2021; Salo et al., 2021). Moreover, the majority of these studies have used induced lesions (Laitinen et al., 2015), neonatal enucleation (Bock et al., 2010) or animal disease models of depression (Khan et al., 2016) or Parkinson's disease (Shimony et al., 2018) as a way of validation. Previous studies conducted in animal models of disorders have used histological techniques showing dMRI measures in GM regions to be sensitive to the underlying pathologies, e.g., neurodegeneration, myelinated fiber loss (Laitinen et al., 2015), and changes in neuronal density (Khan et al., 2016) and fiber density (Shimony et al., 2018). A few other histological validation studies conducted in normal, unaffected gray matter, reported a strong relationship between dMRI measures estimated from DTI, NODDI and constrained spherical deconvolution (CSD) models, and underlying properties of axonal, dendritic, and myelin microstructure in the neuropil (Kroenke et al., 2007; Jespersen et al., 2012; Seehaus et al., 2015; Maiter et al., 2021; Salo et al., 2021).

Even so, gray matter is comprised of not just dendrites and axonal bundles but also cell bodies and extracellular matrix. In GM, cellular composition and organization of cell bodies is very important to study because disorders such as schizophrenia, autism, bipolar disorder, and 22q11.2 deletion syndrome (22q11DS) have been shown to be associated with cytoarchitectural pathologies such as abnormal neuronal migration, changes in cell density, morphology, and other cytoarchitectural abnormalities (Arnold et al., 1991; Avino and Hutsler, 2010; Muraki and Tanigaki, 2015; Cho et al., 2016; Tee et al., 2017; Kikinis et al., 2019; Harrison et al., 2020). So far, there is only one model, the soma and neurite density MRI (SANDI) model, that has primarily focused on the characterization of cellular and neurite densities in gray matter (Palombo et al., 2020). Validation was provided for this model by comparing the SANDI-derived soma fraction in gray matter with the Allen mouse brain atlas contrast that represents the cellular density in the mouse brain (İanuş et al., 2021). However, the SANDI model requires specific acquisition parameters (i.e., very high b-values) which can only be acquired on preclinical or specialized ultra-high gradient strength MRI scanners posing challenges for translation to human application

(Palombo et al., 2020; İanuş et al., 2021). Additionally, it is important to note that in most of the above-mentioned studies conducted in GM, postmortem validation was done using *ex-vivo* dMRI data. Imaging measures derived from the *ex-vivo* dMRI data cannot be directly translated to those measured *in-vivo*. The reason for this lies in the altered properties of the fixed postmortem tissue such as, significantly reduced intrinsic diffusivity and inhomogeneous shrinkage in brain volume due to formalin fixation across brain regions (Siegel et al., 1985; Rane and Duong, 2011; Lerch et al., 2012; Roebroek et al., 2019). These challenges associated with using the *ex-vivo* dMRI data make it difficult to translate the results to *in-vivo* human studies.

A commonly used dMRI model, diffusion tensor imaging (DTI) (Alexander et al., 2007; O'Donnell and Westin, 2011) and a recently developed biexponential model (Rathi et al., 2013; Ning et al., 2015) have been used in several *in-vivo* human studies (especially the DTI model) to understand changes related to normal development, aging, and clinical conditions, showing strong translational value (Kubicki et al., 2007; Lebel et al., 2012; Yoshida et al., 2013; Avram et al., 2016; Wu et al., 2019; Baxi et al., 2020; Le et al., 2020). Measures derived from both these models individually have shown the ability to capture the influence of both genetic and environmental factors on brain microstructure in human subjects (Elman et al., 2017; Vuoksimaa et al., 2017; Gustavson et al., 2019; Baxi et al., 2020). Thus, DTI and biexponential model derived measures once validated, have the potential to be individually used as imaging biomarkers to study disease-related as well as normal development and aging-related brain changes.

The DTI model is by far the simplest and most commonly used model for dMRI data to study brain microstructure in health and disease. The commonly used scalar measures derived from this model are fractional anisotropy (FA) and trace that measure biophysical properties of the underlying tissue. FA measures the degree of anisotropy in the water diffusion within a voxel and trace describes the average mobility of water molecules in the tissue. However, the DTI model relies on the assumption of anisotropic Gaussian diffusion of water molecules in the tissue (Basser et al., 1994; Jones and Cercignani, 2010; O'Donnell and Westin, 2011). In contrast, the biexponential model allows modeling of non-Gaussian water diffusion behavior in complex brain tissue thus making it a more realistic model to probe the complex tissue microstructure (Özarslan et al., 2013; Rathi et al., 2013; Ning et al., 2015). The diffusion propagator derived from the biexponential model uses a mixture of Gaussians (Rathi et al., 2013) to represent the diffusion signal across multiple b -values. In this case, all derived measures have simple analytical expressions, making them easier and more robust to estimate. The scalar measures derived from this biexponential model are mean-squared-displacement (MSD) and return-to-origin-probability (RTOP). MSD primarily captures the displacement

of fast-moving water molecules while RTOP measures the probability of a water molecule returning to its starting position in a given experimental diffusion time and is an indicator of restricted diffusion (Assaf et al., 2002; Wu and Alexander, 2007; Özarslan et al., 2013; Ning et al., 2015; Boscolo Galazzo et al., 2018; Afzali et al., 2021). For example, if water is highly restricted, one might expect higher RTOP as there is a higher likelihood of the water molecules coming back to their starting positions. On the other hand, in the ventricles where there is little restriction, the RTOP is low. Similarly, MSD will be high in the ventricles and lower in restricted regions.

However, the question of how the fundamental GM microstructural properties such as cell size, cell packing density, spatial arrangement, and geometry of cell bodies influence these measures (FA, Trace, MSD and RTOP) derived from these two *in-vivo* dMRI models (DTI and Biexponential), still remains unclear. Quantifying the connection between these dMRI measures and histological properties of cellular architecture is critical for progress in the field and is the main focus of this work.

Therefore, in this study, we investigated how the underlying cytoarchitecture in gray matter is related to DTI and biexponential measures. To validate these diffusion measures (trace, FA, MSD and RTOP), we compared them with the histology based cytoarchitectural regional tissue properties of average and heterogeneity of cell area density. Specifically, we used digitized Nissl-stained slices and *in-vivo* high-resolution multi-shell dMRI data acquired from the same four monkeys to quantify the contribution of underlying cytoarchitecture to the dMRI measures.

Methods

Demographics

This study included *in-vivo* MRI scans and archived brain tissue from four rhesus monkeys (all male) 19–20 years old (equivalent to 57–60 years in humans; Tigges et al., 1988). A small age range was chosen specifically to reduce age effect on variability across the histological and imaging measures. Health records of these monkeys were screened to exclude any possible confounding clinical diseases or experimental manipulations that could impact normal aging.

Monkeys were obtained from national primate research facilities or private vendors and had known birth dates and complete health records. Monkeys were housed in the Animal Science Center of Boston University School of Medicine which is AAALAC accredited. All procedures were approved by the Boston University Institutional Animal Care and Use Committee and complied with the NIH guidelines for the care and use of laboratory animals.

Structural and diffusion MRI

MRI acquisition

Structural and diffusion MRI scans were acquired using the same protocol and scanner for all four monkeys as described below. Monkeys were anesthetized with ketamine (10 mg/kg) and xylazine (0.10 mg/kg) and placed into a 3 Tesla Connectome MRI scanner (Siemens), located at the Martinos Center for Biomedical Imaging using an MRI compatible stereotactic frame that fixed the monkey head in the standard coronal plane (Saunders et al., 1990). The following parameters were used for acquiring structural (sMRI) and dMRI scans, which took around 3 h:

<i>T1</i>	<i>MPRAGE</i>	<i>Structural</i>	<i>MRI:</i>
TI/TR/TE =	1100/2530/1.37 ms,	flip angle =	7°,
FOV =	160×160 mm ² ,	slices =	176,
voxel size =	0.6×0.6×0.59 mm ³ ,	bandwidth =	650 Hz/pixel,
32 channel head coil,	and acceleration factor of 2.		

Multi-shell Diffusion-weighted MRI: Spin-echo single-shot EPI sequence, TR/TE = 15700/73 ms, flip angle = 90°, slices = 118, FOV = 140×140 mm², voxel size = 0.8×0.8×0.8 mm³, bandwidth = 1185 Hz/pixel. Three repetitions of diffusion MRI scans were acquired with 11 b-value of 0 s/mm² and 60 directions for each b-value of 1,000, 2,000, and 3,000 s/mm².

MRI preprocessing

MRI scans were preprocessed using the standard in-house pipeline (<https://github.com/pnlbwh>) (Figure 1). Both sMRI and dMRI image modalities were visually inspected for significant artifacts and signal dropouts. Upon manual visual inspection of dMRI data, we observed that one of the three repetition scans from two monkeys, each had significant motion artifacts through most volumes and hence if one or more slices had motion artifacts the corresponding dMRI volume was removed from further processing. No data was removed from the remaining repetition scans as we were able to correct for minor motion artifacts. This data can be made available upon request.

Diffusion-weighted MRI scans: Diffusion MRI scans for each monkey included three repetitions/runs which went through the following preprocessing steps (Figure 1) that included MP-PCA denoising (Veraart et al., 2016) using https://github.com/NYU-DiffusionMRI/mpcca_denoise code, followed by motion correction, brain extraction and eddy current correction using Functional Magnetic Resonance Imaging of the Brain (FMRIB) Software Library (FSL) software (<http://www.fmrib.ox.ac.uk/fsl>) (Smith et al., 2004) on each run. The three preprocessed runs were then averaged into one volume for each monkey.

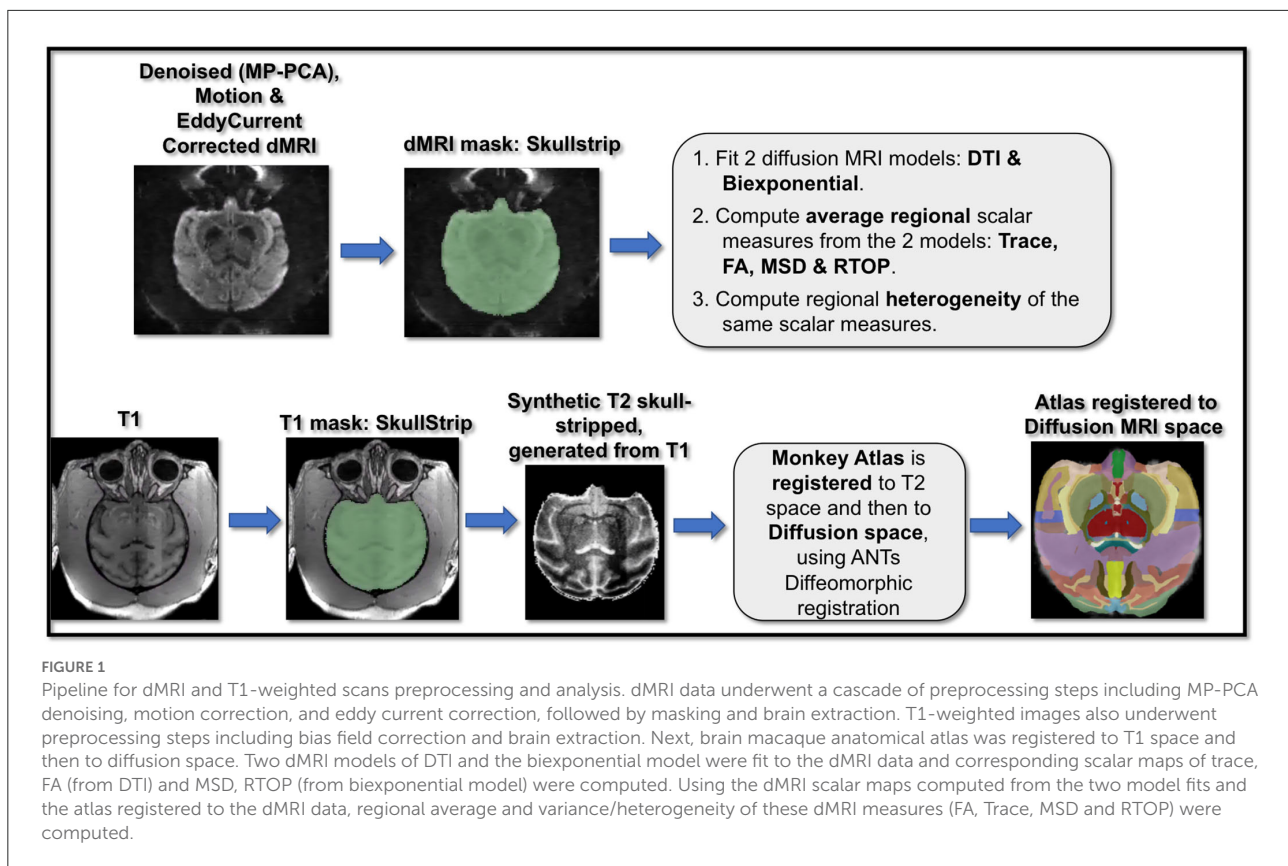
T1-weighted scans: T1-weighted scans went through the preprocessing steps (Figure 1) that included skull stripping

and bias field correction using FSL (Smith, 2002). Next, T2-weighted images were synthetically generated using in-house MATLAB scripts that performed a cascade of image processing steps including intensity reversal, log transformation for image enhancement and histogram equalization on preprocessed T1-weighted scans (Kubicki et al., 2019). T2-weighted images were generated for accurate co-registration of the T1-weighted images and associated brain parcellation with dMRI data (as the intensities of T2-weighted and b = 0 dMRI images are quite similar). In order to calculate regional diffusion MRI measures, a brain macaque atlas (Dubach and Bowden, 2009; Rohlfing et al., 2012) was non-linearly registered first to the T2-weighted images and then to the diffusion space for each monkey, using Advanced Normalization Tools (ANTs) registration (Avants et al., 2014).

Fitting diffusion MRI models

DTI Model: Conventional diffusion tensor imaging (DTI) model was fit using Slicer v4.8 (<http://www.slicer.org>), (Fedorov et al., 2012) to diffusion MRI data using the b = 0 and b = 1000 s/mm² shells of the multi-shell diffusion MRI scans. DTI model is a single tensor model and relies on the assumption that water diffusion in the brain follows a mono-exponential Gaussian distribution (Basser et al., 1994; Jones and Cercignani, 2010). Using this DTI model, scalar maps of fractional anisotropy (FA) and trace (Tr) were computed for each monkey. FA represents the degree of anisotropy of the biological tissue and has been commonly used to study white matter structure. Trace describes the average mobility of water molecules in the tissue.

Biexponential model: A more sensitive model, i.e., biexponential model was fit to the multi-shell dMRI data, which allows modeling of non-Gaussian water diffusion behavior in brain tissue exhibited by the underlying biological structures e.g., myelin, cell bodies and its processes (Özarslan et al., 2013; Rathi et al., 2013; Baxi et al., 2020). The model consisted of a weighted mixture of two exponentials oriented in the same direction modeling the signal across multiple b-values and gradient directions (Mulkern et al., 1999; Rathi et al., 2013). CSF contamination was accounted for and removed when we modeled the diffusion behavior using the biexponential model. This model consisted of an isotropic compartment to model the CSF contamination apart from the restricted compartment to model the non-gaussian diffusion in the GM tissue for each voxel. This allowed us to remove CSF contamination before computing the dMRI measures used in further analysis. More details on this model can be found in a recently published paper by Baxi et al. (2020). Scalar maps of return-to-origin-probability (RTOP) and mean squared displacement (MSD) were then computed for each monkey using this biexponential model (Ning et al., 2015; Baxi et al., 2020). MSD primarily captures the displacement of fast-moving water molecules (i.e., it is more sensitive to larger displacements).



Immunohistochemistry

Macaque postmortem tissue processing and histology

The four monkeys that were scanned *in-vivo* to acquire dMRI scans, were sacrificed shortly after the MRI scans. They were deeply anesthetized with sodium pentobarbital and perfused transcardially through the aorta with Krebs Henseleit buffer, pH 7.4 at 4°C for 5 min while fresh tissue samples were harvested. This was followed by perfusion with 4% buffered paraformaldehyde (pH 7.4, 37°C) for 10 min. Next, the brain was blocked, *in situ*, in the coronal stereotactic plane, removed from the skull and placed in the same paraformaldehyde fixative overnight at 4°C. It was then cryoprotected by incubations in 0.1 M phosphate buffer containing first 10% glycerol with 2% DMSO and then 20% glycerol and 2% DMSO (Rosene et al., 1986). Next it was flash frozen in isopentane at -75°C and stored at -80°C. Frozen sections were cut into interrupted series on a sliding microtome. Eight sections were cut at 30 μm thickness and one at 60 μm and this was repeated until the entire whole hemisphere brain was cut. As a result, sections within each series are spaced at 300 μm intervals. The 60 μm sections were mounted onto gelatin-albumin subbed microscope slides, dried overnight at room temperature and then stained with thionin to reveal cell bodies. This series was prepared for

digitization as done here and for stereology which is more efficient with the thicker sections. The other 8 series of 30 μm sections are collected in phosphate buffer with 15% buffered glycerol and stored at -80°C until needed for other staining such as immunohistochemistry (IHC) (see Estrada et al. (2017) for examples). No 30 μm IHC series were analyzed for this study.

Microscopy digitization

We then digitized the stained slices by imaging them using a Zeiss Axioscan microscope with 10x objective to obtain Z-stacked images which were then merged into a single image per slice with resolution of 0.44 × 0.44 μm². Z-stack imaging of tissue samples, allows for accurate visualization of the cell bodies in the tissue.

Cell segmentation of digitized histological slices

To avoid registration errors between histology and dMRI, we used manual delineations of nine cortical and subcortical regions on histology sections. We then segmented the histological slices to identify stained cell bodies using the MATLAB Image Processing Toolbox and Nuclei Counter Code (<https://www.mathworks.com/matlabcentral/fileexchange/>

45174-nuclei-counter) (Figure 2). The segmentation quality of our code was assessed by comparing the automatically segmented samples with the manually segmented samples (performed by trained expert). Three samples were chosen randomly from the anterior, middle, and posterior sections of each ROI. Measures of Dice coefficient and error in cell area density were computed for each of these samples upon comparing the automated cell segmentation with the manual cell segmentation.

Computing average and heterogeneity regional measures

The distribution profile of diffusion measures and histological cytoarchitectural properties of cell composition in any brain region should be described by two metrics, mean/average and variance/heterogeneity, as opposed to just the mean/average which is commonly done. This is because two very differently shaped distribution profiles as seen in Figure 3 could have similar means and using only the mean to characterize a distribution profile would give the false impression of the distributions being similar when they might be different in their variance.

Since cortex is highly plastic and undergoes changes in cellular composition with age, this could alter the spatial organization of GM within a voxel and hence change heterogeneity measures (Zatorre et al., 2012; Rathi et al., 2014). The importance of using variance/heterogeneity to study the structure has also been shown by previous studies to differentiate between patients with early course schizophrenia and healthy controls (Seitz et al., 2018) and to study/detect disruption of migration patterns of neural crest cells in 22q11DS (Kikinis et al., 2019).

Hence, in this study, we computed both mean/average and variance/heterogeneity of dMRI and histological measures for nine gray matter regions. It is well known from neurobiology literature (Brodman, 1909; Vogt and Vogt, 1926; Goldman-Rakic, 1982) that different brain areas including cortical and subcortical regions, vary in their cellular composition and organization across different gray matter regions. The nine GM ROIs used in this study (Figure 4), were chosen to get a good sampling of different cytoarchitectural properties. Hence it included cortical regions of anterior cingulate gyrus (ACG), precentral gyrus, postcentral gyrus, superior temporal gyrus (STG), insular cortex and entorhinal cortex along with subcortical regions of caudate, putamen, and thalamus.

Estimating regional average and heterogeneity dMRI measures

The brain macaque atlas (Dubach and Bowden, 2009; Rohlfing et al., 2012) was registered to the dMRI scans for

each monkey which was used to compute regional average (avgdMRI_{meas}) and heterogeneity (hdMRI_{meas}) of dMRI measures for nine GM regions of interest (ROIs). These measures were computed using FA, trace, MSD and RTOP for each monkey. AvgdMRI_{meas} was computed by taking the average of a given dMRI measure (FA/trace/MSD/RTOP) over all voxels in an ROI. HdMRI_{meas} is defined as the inter-voxel variance in a given dMRI measure (FA/trace/MSD/RTOP) across a region.

$$\text{avgdMRI}_{meas} = \frac{1}{N} \times \sum_{i=1}^N \text{dMRI}_{meas_i}$$

N is the number of voxels in the ROI and the dMRI measure in a voxel is indexed by i.

$$\text{hdMRI}_{meas} = \frac{1}{N^2} \times \sum_{i=1}^N \sum_{j=1}^N \|\text{dMRI}_{meas_i} - \text{dMRI}_{meas_j}\|$$

N is the number of voxels in an ROI and the dMRI measure in a voxel is indexed by i or j.

Estimating regional average and heterogeneity histological measures

Next, we computed analogous histological measures of cell area density and heterogeneity of cell area density for the same 9 ROIs for each monkey, to compare with regional average and heterogeneity of dMRI measures (Figure 5). Cell Area Density for each region was computed as the fraction of area covered by cell bodies in each ROI. In order to compute the heterogeneity of cell area density, each ROI was resampled into 2D grid to match the diffusion voxel size. Variance of cell area density was then computed across all such 2D voxel-sized squares within each ROI, which provided us the heterogeneity in cell area density.

Comparing *in-vivo* dMRI measures with *ex-vivo* histology measures

In order to quantify the contribution of regional histological measures to the dMRI measures (FA/trace/MSD/RTOP), we conducted Pearson correlations between histology-derived and dMRI-derived measures (Figure 5). We performed correlations between average histology and dMRI measures separately in cortical and subcortical regions, given the major cytoarchitectural differences known to exist between cortical and subcortical regions (Amunts and Zilles, 2015). All *p*-values were corrected for multiple comparisons using FDR-correction. We also checked for the effect of regional volume on regional average cell area density and did not find any significant effect.

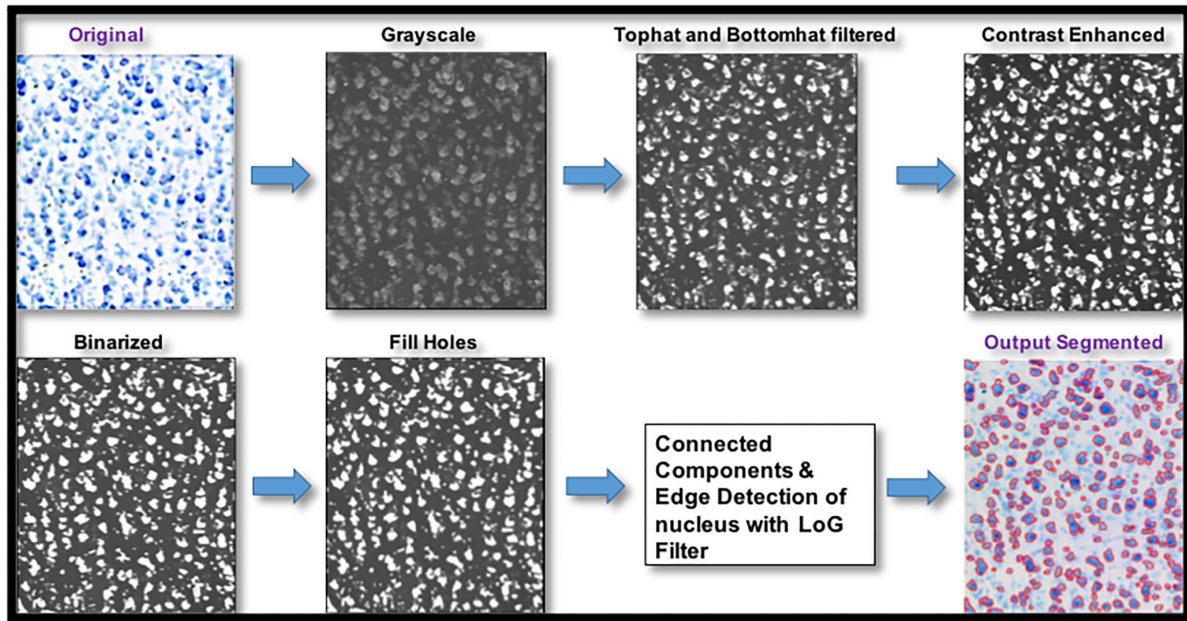


FIGURE 2
 Pipeline for digitized histological sections preprocessing and cell segmentation. Digitized histological section images underwent preprocessing steps that involved top hat and bottom hat filtering, contrast enhancement, binarizing the image using a histogram-based threshold, filling holes followed by connected-component labeling for cell segmentation and edge detection with Laplacian of gaussian filter for plotting the edges of the cell bodies.

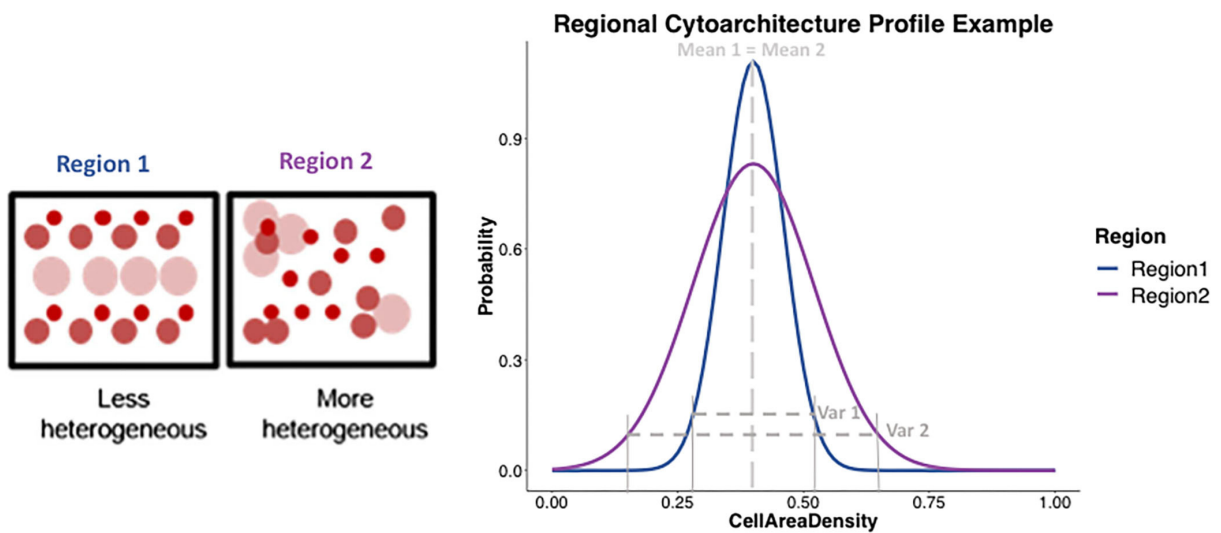
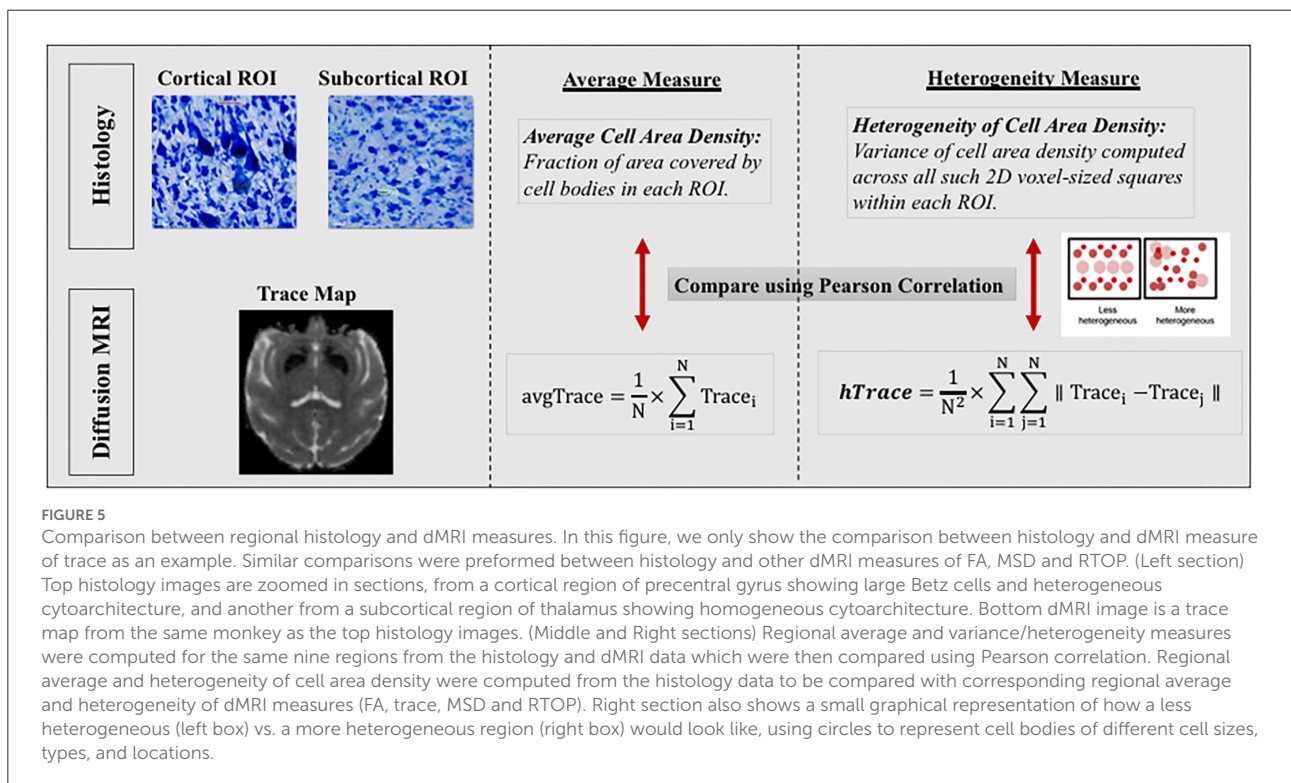
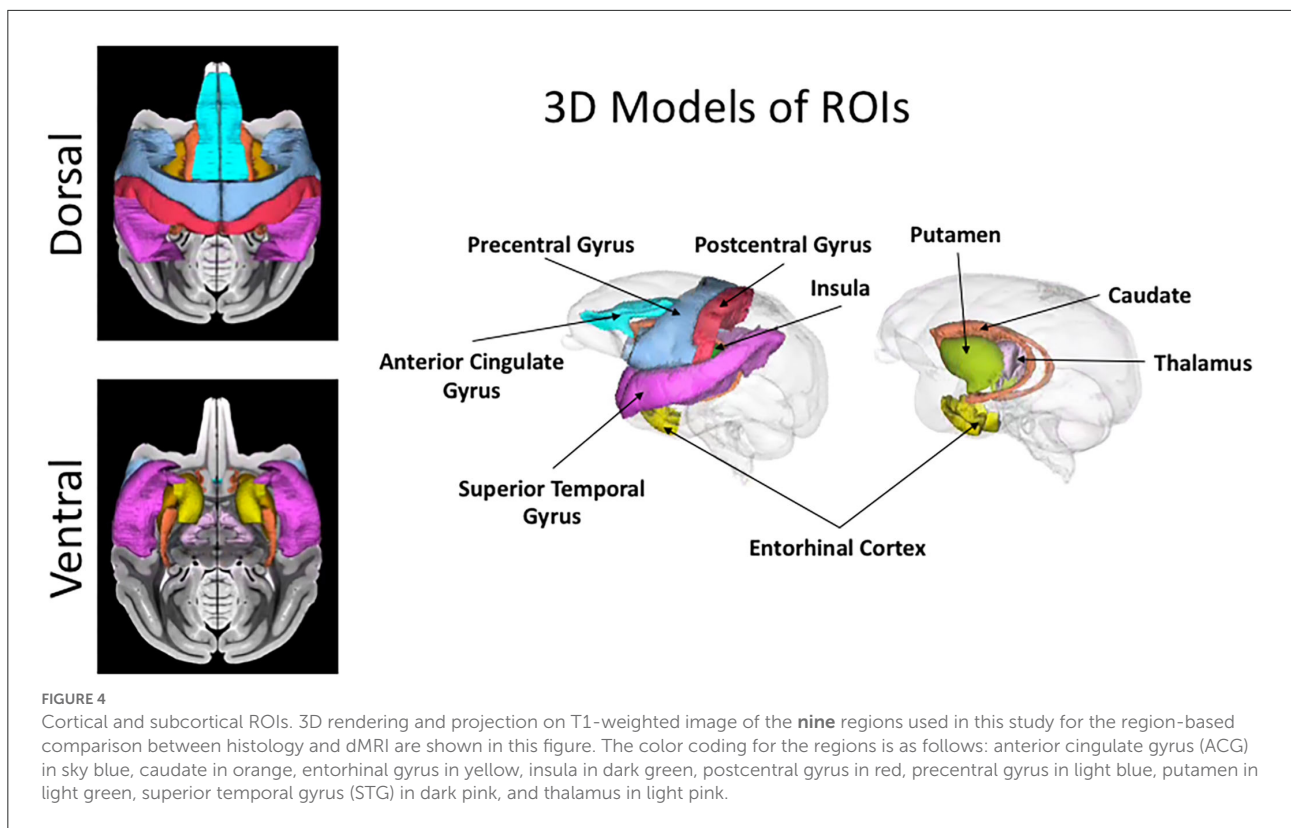


FIGURE 3
 Example representation of the cytoarchitecture profile in different gray matter regions. (Left) Two boxes represent two regions, with circles representing cell bodies of different types, sizes, and uniformly or non-uniformly packed, showing region 1 (blue) being less heterogeneous and region 2 (purple) being more heterogeneous in the underlying cytoarchitecture. (Right) Plot shows an example of what the cytoarchitecture profile would be expected to look like for region 1 (blue) and region 2 (purple) using two different shaped distributions. Region 1 being less heterogeneous, would be expected to show a distribution profile (in blue) that has a certain mean and a tighter variance. On the other hand, a more heterogeneous region 2 would be expected to show a distribution profile (in purple) with similar mean but a much larger variance than region 2. The shape of the two-distribution profile for region 1 and region 2 can be seen to be described by both mean and the variance.



Results

Cell segmentation algorithm quality assessment

Quality of our automated cell segmentation was assessed by comparing the automatically segmented samples with the manually segmented samples that were chosen from the anterior, middle, and posterior sections of each ROI. Quantitative measures of dice overlap coefficient and error in cell area density were computed for each sample. Dice coefficient provides the similarity index between two segmentations and ranges from 0 to 1, with 1 signifying an absolute match. Samples from all three portions of all the ROIs showed high dice coefficient which varied between 0.91 and 0.99, and an average error in the estimated cell area density measure of less than 0.04.

Comparing DMRI (*in-vivo*) measures with histology (*ex-vivo*) measures

Comparison between dMRI measures (DTI and biexponential model) and corresponding histology measures of cell area density computed for 9 GM regions from four rhesus macaques, showed the following results.

Average regional measures

Average cell area density values which were computed as the fraction of area covered by all cell bodies (Figure 6) were overall consistent with the previous studies (Semendeferi et al., 2001; Casanova et al., 2002) that measured Gray Level Index (GLI) which is defined as the fraction of the area covered by Nissl-stained neurons and glial cells in postmortem samples. Gray level index is thus the same as the average cell area density defined in this study. Average trace showed significant positive correlation with average cell area density in cortical regions ($r = 0.47$, $p = 0.02$), whereas it showed significant negative correlation in subcortical regions ($r = -0.71$, $p = 0.0097$) (Figure 6). Similarly, between average cell area density and average MSD, results showed a positive correlation in cortical regions ($r = 0.64$, $p = 0.00076$), whereas a negative correlation was shown in subcortical regions ($r = -0.7$, $p = 0.011$) (Figure 6). Average FA when correlated with average cell area density did not show significant correlation in cortical regions ($r = -0.36$, $p = 0.082$) but showed positive correlation in subcortical regions ($r = 0.74$, $p = 0.0062$) (Figure 6). Average RTOP did not show significant correlation ($p > 0.05$) with average cell area density in either cortical or subcortical regions. Variability in the histology and dMRI measures within each region can be observed across the four monkeys (same colors on Figure 6) showing the sensitivity to inter-subject differences in the brain structure. Even though measures for each region

from all four monkeys show some variation, they tend to cluster together, highlighting the robustness of our results across monkeys.

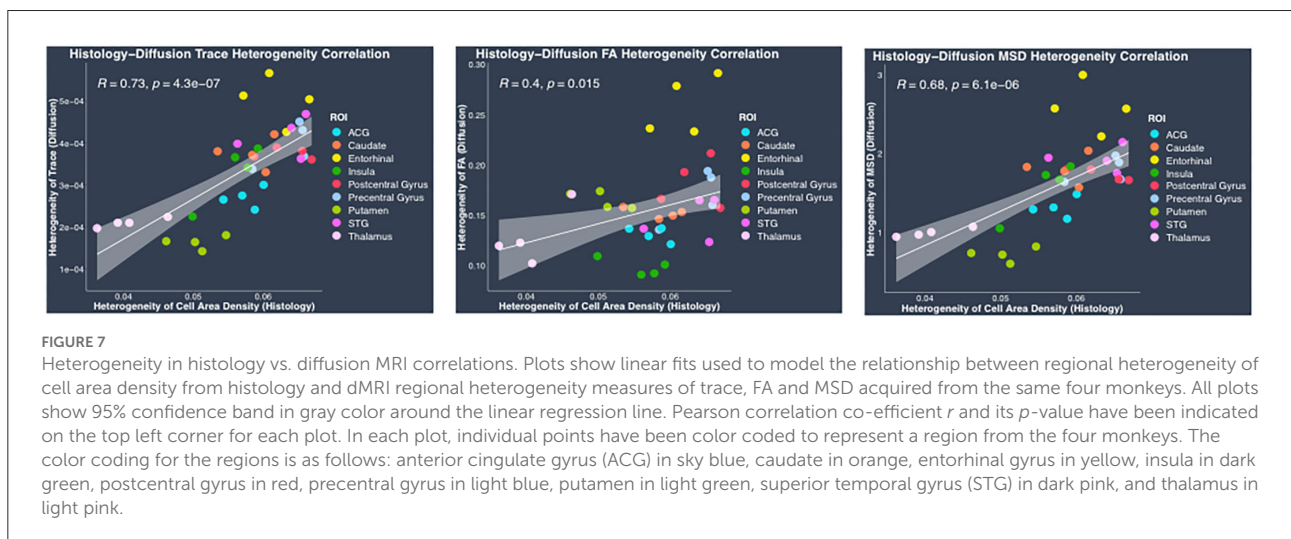
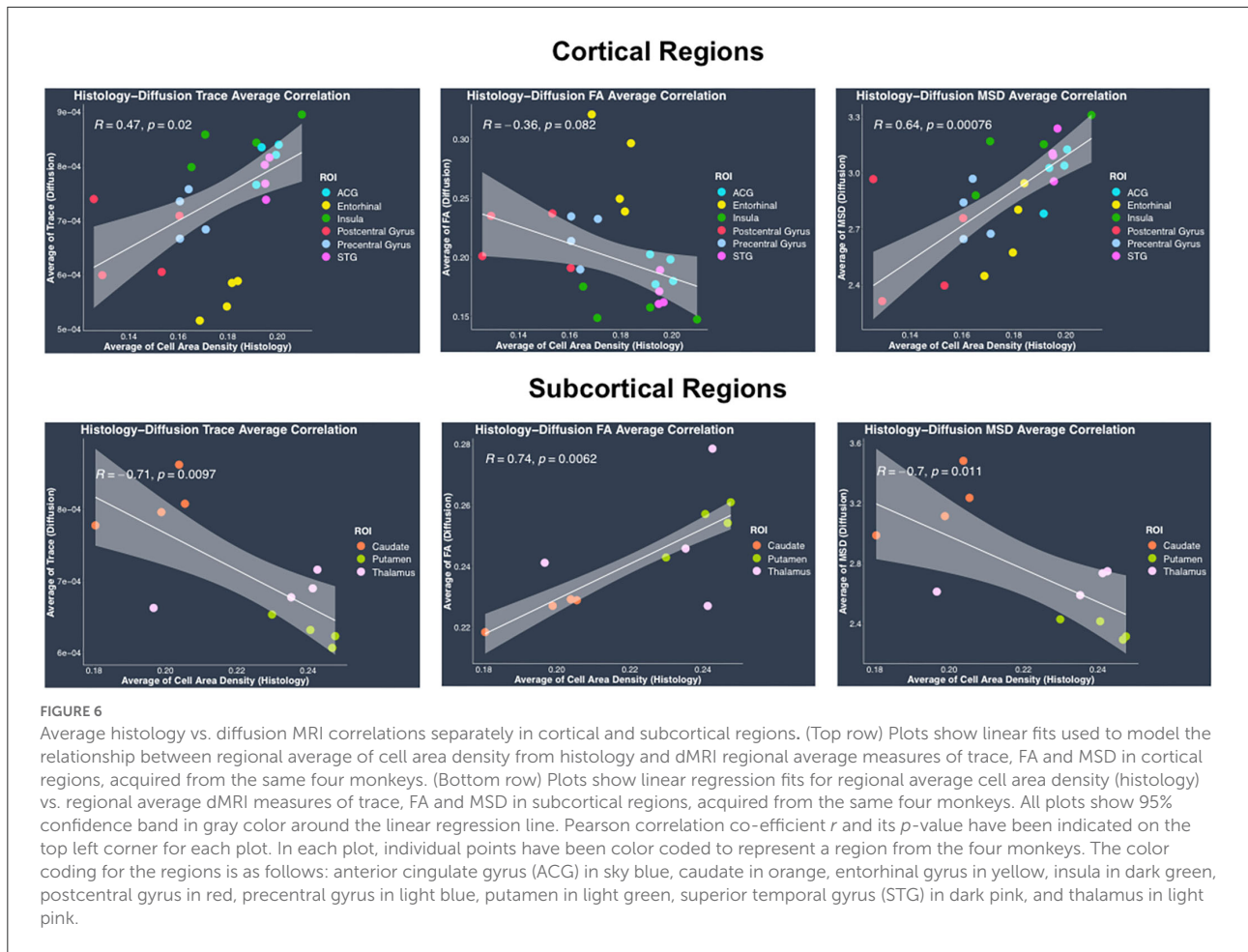
Heterogeneity regional measures

Regional heterogeneity in cell area density measure computed from histology data showed a high positive significant correlation with DTI-derived hTrace ($r = 0.73$, $p = 4.3 \times 10^{-7}$) and biexponential model-derived hMSD ($r = 0.68$, $p = 6.1 \times 10^{-6}$) measures and moderate correlation with DTI-derived hFA ($r = 0.4$, $p = 0.015$) (Figure 7). No significant correlation was observed between the histological measure of regional heterogeneity in cell area density measure and biexponential model-derived hRTOP ($p > 0.05$) (Figure 7). We also performed correlations between heterogeneity histology and dMRI measures separately in cortical and subcortical regions, which showed similar trends as the results upon combining cortical and subcortical regions in the same analysis. Overall, these results showed that the higher the heterogeneity in cell area density, the higher the heterogeneity in trace and MSD (and FA to a smaller degree).

Discussion

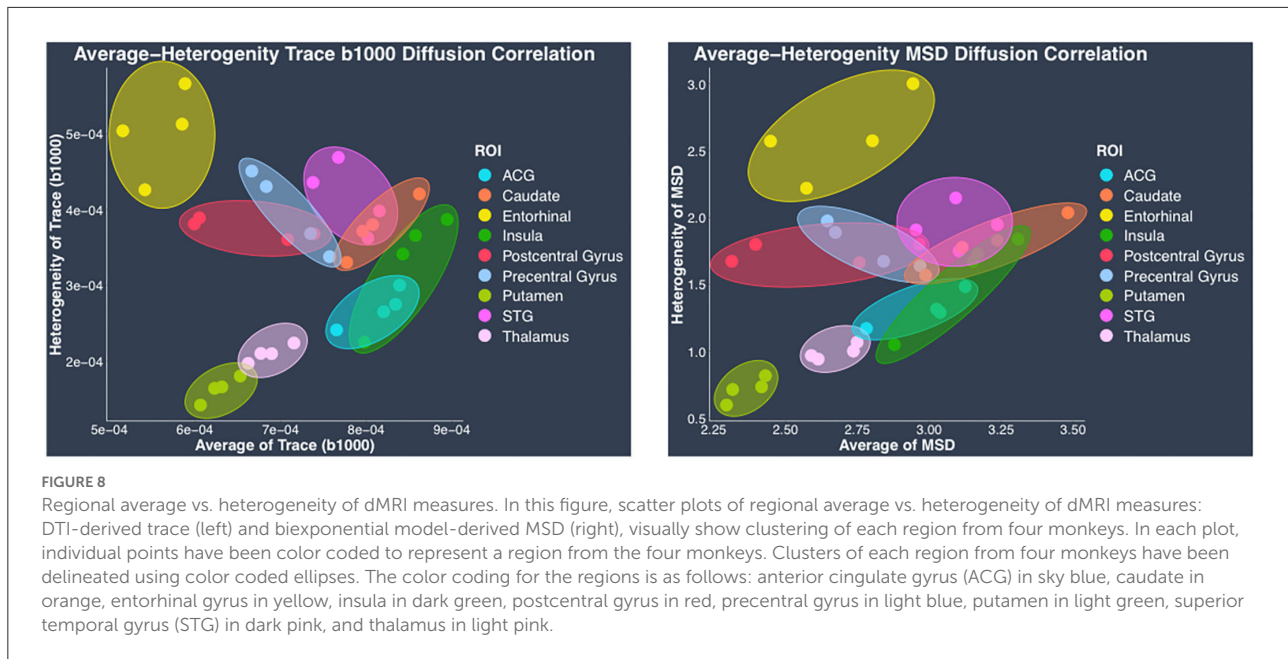
This study presents an important step toward quantifying the contribution of GM cytoarchitecture to *in-vivo* dMRI measures using histology in rhesus monkeys. This research paves the way for bridging the gap between the two distinct modalities and allows for a better and more informed use of dMRI in the future. Specifically, we aimed to investigate the influence of the underlying cell composition and spatial organization/distribution on dMRI measures estimated using the conventional DTI model (FA and trace) and an advanced biexponential model (MSD and RTOP). This was achieved by conducting correlations between regional average and heterogeneity of cell area density (estimated using Nissl-stained digitized histology data) and corresponding dMRI measures (FA, trace, MSD and RTOP), in the same four rhesus monkeys. The work presented here is based on *in-vivo* dMRI in non-human primate animal models and provides an important guide to interpreting the results of *in-vivo* dMRI measures in the human brain (Gao et al., 2013). The main finding of this study is that regional heterogeneity in trace and MSD measures from dMRI capture the underlying biological features of spatial arrangement of cell bodies as measured by heterogeneity of cell area density in that region.

Our results showed a statistically significant positive correlation between the histological measure of regional heterogeneity in cell area density and dMRI heterogeneity measures of trace and MSD. This suggests that the dMRI heterogeneity measures are sensitive to heterogeneity in the cell



area density, driven by the variability in cell size and cell packing density in a region. A region is considered to be homogeneous in cytoarchitecture if the variation in the cell size and type is low

and they are uniformly distributed across the region. Conversely, a region with cell bodies of varied sizes and shapes organized in a complex, non-uniform arrangement is considered to have a



heterogeneous cytoarchitecture. Our findings show that hTrace and hMSD can capture the variability in the underlying cell composition and spatial arrangement.

GM regions are known to vary in their underlying cytoarchitecture, with some regions exhibiting more heterogeneity in the organization of cell bodies and its processes compared to others. Our results reflect these differences between regions. For example, the entorhinal cortex shows the highest heterogeneity in trace and MSD and also in heterogeneity in cell area density, as compared to their cortical and subcortical regions. This finding corroborates with previous postmortem studies reporting the complex cytoarchitectonic organization of the entorhinal cortex, which can be further differentiated into seven subfields on the basis of differences observed in the morphological features visible in Nissl- and fiber-stained preparations (Amaral et al., 1987; Swards and Swards, 2003). These studies found that rostrally located fields show a number of morphological inhomogeneities with neurons organized in patches in contrast to the caudally located subfields that more closely resemble the neocortex with neurons arranged in discrete radial columns (Amaral et al., 1987; Swards and Swards, 2003; de Góis Morais et al., 2020). Heterogeneity in cell area density observed in precentral gyrus and postcentral gyrus can be attributed to the presence of large pyramidal cells (Betz cells), in the layer V of precentral gyrus as well as somatotopic organization (Cusick et al., 1989; Krubitzer and Kaas, 1990; Fink et al., 1997; Eickhoff et al., 2007). Among the subcortical regions, our results show that caudate shows higher heterogeneity in cytoarchitecture as compared with putamen, which is consistent with a previous study that reported homogeneous cellular appearance of the putamen compared to the more prominent

complex cellular islands consisting of densely packed neurons of variable cell sizes and shapes seen in the caudate nucleus (Goldman-Rakic, 1982).

Further, our results demonstrate that the dMRI measures of hTrace, hFA, hMSD and hRTOP show differences in their ability to capture the biological features of the underlying cytoarchitecture. Both hMSD and hTrace show similar high positive correlation with the histology measure of heterogeneity in cell area density. This could be explained by the similarities in the biophysical properties captured by these two measures derived from DTI and biexponential models. Previous studies have shown that MSD and trace measures are related *via* the Einstein diffusion equation (Wu and Alexander, 2007; Hosseinbor et al., 2013; Boscolo Galazzo et al., 2018) and have been reported to show visually correlated behavior with very similar tissue contrast maps (Wu and Alexander, 2007) and similar patterns when studied in patients with ischemic oedema (Alexander et al., 2007). These studies are thus consistent with our finding of similar patterns seen in the correlations between both hMSD and hTrace with heterogeneity in cell area density. However it is important to note that previous studies have also found MSD to be more sensitive to underlying microstructure as compared to trace, demonstrating the advantage of using the biexponential model measure of MSD (Boscolo Galazzo et al., 2018). In contrast to the findings from MSD and trace, hFA showed only low to moderate influence of heterogeneity in cell area density. FA is known to measure the restriction and anisotropy of water diffusion and, in WM it has been shown to capture the underlying biological properties of myelin integrity and axonal architecture (Alexander et al., 2007; O'Donnell and Westin, 2011). Even in GM, postmortem validation studies have

shown that orientation and distribution of myelin and axons significantly contribute to FA (Kroenke et al., 2007; Jespersen et al., 2012; Seehaus et al., 2015). Since our histology data did not contain myelin stains, it is not surprising that there is only a low to moderate correlation with cell composition observed relative to FA. It is likely that similar to FA, the biological factors of myelin and axons could also be a major contributor to RTOP which is not captured by our Nissl-stained cell bodies and could be the reason why our study found no significant contribution of cell composition on RTOP and should be investigated in future studies.

In contrast to the regional heterogeneity dMRI measures, the regional average dMRI measures estimated from both DTI and the biexponential model did not show significant correlation with the histological measure of regional average cell area density when all the regions (cortical and subcortical) were included together in the correlation analysis. However, separate analysis conducted in cortical and subcortical regions revealed opposite trends showing positive correlation between average trace, MSD, and average cell area density in cortical regions whereas negative correlation in subcortical regions. These opposing correlation trends observed between average trace, MSD, and average cell area density in cortical vs. subcortical regions, could explain the reason why we did not see any significant correlation when including all the regions (cortical and subcortical) together in the analysis. Future studies with data from more subcortical regions and perhaps myelin, dendrites, axonal, and cell type specific stains are needed to understand the reason behind such opposing correlation trends observed between the average dMRI and histology measures in cortical vs. subcortical regions. Nevertheless, our results show that regional average dMRI measures of trace and MSD are sensitive to the underlying biological feature of average cell area density. Additionally, the two-dimensional scatter plots of DTI-derived trace measure (hTrace vs. avgTrace) and biexponential-derived MSD measure (hMSD vs. avgMSD) (Figure 8), both showed that the same regions from all four monkeys visually clustered together.

Clustering of the same regions from all four monkeys demonstrates that average and heterogeneity dMRI measures together show regional specificity, suggesting sensitivity to microstructural tissue properties. It is important to note that in this study we only investigated the histological measure of cell composition, and it is possible that other biological features of myelin, axons, and dendrites are the likely contributors to the dMRI measures.

Future implications

Investigation of the contribution of underlying cytoarchitecture to the dMRI measures, provided us with the much needed validation for dMRI measures of trace

and MSD regarding their ability to capture changes in cell composition and organization in GM. Changes in cell density and cell size as well as position due to cell migration, have been observed during development and aging (Götz et al., 2016; Martínez-Pinilla et al., 2016; Nakafuku and Del Águila, 2020; d'Alessandro et al., 2021; Sikora et al., 2021). Non-invasive imaging measures of hTrace, hMSD along with average trace, and average MSD could be used as important tools in future longitudinal research studies investigating GM changes during normal development and aging. In addition, abnormalities in the cellular microstructure have been reported in relation to several developmental as well as degenerative disorders such as autism, schizophrenia, Alzheimer's, and Parkinson's (Arnold et al., 1991; Cho et al., 2016; Martínez-Pinilla et al., 2016; Giguère et al., 2018). Our measures of MSD and trace could thus prove extremely valuable biomarkers in the diagnosis and treatment monitoring of such disorders.

Limitations

This study has a few limitations that must be acknowledged. We acknowledge that other biological factors such as synaptic changes (synaptogenesis, pruning) or changes in dendritic arborization, myelination, axonal orientation could also influence dMRI measures, which should be investigated in future work. In addition, our histological study used spaced sections forcing our analysis to be conducted on 2D sections within a region, leading to local discontinuities. In the future, methods such as CLARITY that allow conducting histological measurements in whole intact tissue followed by 3D imaging could be used for validation of dMRI-based microstructure estimates. Nevertheless, this study is an important first step toward histological validation of dMRI measures in GM in macaque.

Conclusion

Based on the results of our study we conclude that dMRI measures can serve as imaging biomarkers of GM cellular structure and organization. Average and heterogeneity in dMRI measures of trace and MSD appear to be best suited to study the underlying cytoarchitecture. Direct quantitative comparisons conducted in this study between these dMRI measures and histological features of cytoarchitecture would provide an important guide to interpreting the results of studies using these dMRI model-derived measures. These dMRI measures of hTrace, hMSD, average trace and average MSD thus have the potential for use as non-invasive imaging biomarkers in studies that involve investigation of the changes in GM cytoarchitecture related to development and aging in

healthy populations as well as abnormal cellular pathologies in clinical studies.

Data availability statement

The raw data supporting the conclusions of this article will be made available by the authors, without undue reservation.

Ethics statement

The animal study was reviewed and approved by Boston University Institutional Animal Care.

Author contributions

MK and YR contributed to the conception and design of the study as well as supervised and provided inputs throughout the study. GP, BJ, and AK scanned the animals and acquired the imaging data. NM provided inputs related to neuroanatomy during the interpretation of results and drawing of the anatomical regions. DR and TM harvested the tissue samples upon sacrificing the same animals and conducted immunohistochemistry. SC-K contributed to the image analysis. MB digitized the stained histology slices, performed image and statistical analysis as well as wrote the article. All authors read the manuscript, contributed to the revision and approved the submitted version.

References

- Afzali, M., Pieciak, T., Newman, S., Garyfallidis, E., Özarslan, E., Cheng, H., et al. (2021). The sensitivity of diffusion MRI to microstructural properties and experimental factors. *J. Neurosci. Methods* 347, 108951. doi: 10.1016/j.jneumeth.2020.108951
- Alexander, A. L., Lee, J. E., Lazar, M., and Field, A. S. (2007). Diffusion tensor imaging of the brain. *Neurotherapeutics* 4, 316–329. doi: 10.1016/j.nurt.2007.05.011
- Amaral, D. G., Insausti, R., and Cowan, W. M. (1987). The entorhinal cortex of the monkey: I. cytoarchitectonic organization. *J. Comp. Neurol.* 264, 326–355. doi: 10.1002/cne.902640305
- Amunts, K. and Zilles, K. (2015). Architectonic mapping of the human brain beyond Brodmann. *Neuron* 88, 1086–1107. doi: 10.1016/j.neuron.2015.12.001
- Arnold, S. E., Hyman, B. T., Van Hoesen, G. W., and Damasio, A. R. (1991). Some cytoarchitectural abnormalities of the entorhinal cortex in schizophrenia. *Arch. Gen. Psychiatry* 48, 625–632. doi: 10.1001/archpsyc.1991.01810310043008
- Assaf, Y., Ben-Bashat, D., Chapman, J., Peled, S., Biton, I. E., Kafri, M., et al. (2002). High b-value q-space analyzed diffusion-weighted MRI: application to multiple sclerosis. *Magn. Reson. Med.* 47, 115–126. doi: 10.1002/mrm.10040
- Avants, B. B., Tustison, N. J., Stauffer, M., Song, G., Wu, B., Gee, J. C., et al. (2014). The Insight ToolKit image registration framework. *Front. Neuroinform.* 8, 44. doi: 10.3389/fninf.2014.00044
- Avino, T. A. and Hutsler, J. J. (2010). Abnormal cell patterning at the cortical gray–white matter boundary in autism spectrum disorders. *Brain Res.* 1360, 138–146. doi: 10.1016/j.brainres.2010.08.091
- Avram, A. V., Sarlls, J. E., Barnett, A. S., Özarslan, E., Thomas, C., Irfanoglu, M. O., et al. (2016). Clinical feasibility of using mean apparent propagator

Funding

We gratefully acknowledge the funding provided by following grants: RO1 AG042512 National Institute on Aging (PI: MK, NM, and DR); RF1 AG043640 (PI: DR). R01 MH111917 National Institute of Mental Health (PI: YR); R01 MH102377 National Institute of Mental Health (PI: MK); R01 MH112748 National Institute of Mental Health (PI: MK and NM); R01 MH119222 National Institute of Mental Health (PI: YR); K24 MH110807 National Institute of Mental Health (PI: MK).

Conflict of interest

The authors declare that the research was conducted in the absence of any commercial or financial relationships that could be construed as a potential conflict of interest.

Publisher's note

All claims expressed in this article are solely those of the authors and do not necessarily represent those of their affiliated organizations, or those of the publisher, the editors and the reviewers. Any product that may be evaluated in this article, or claim that may be made by its manufacturer, is not guaranteed or endorsed by the publisher.

(MAP) MRI to characterize brain tissue microstructure. *Neuroimage* 127, 422–434. doi: 10.1016/j.neuroimage.2015.11.027

Baek, S.-H., Park, J., Kim, Y. H., Seok, H. Y., Oh, K.-W., Kim, H. J., et al. (2020). Usefulness of diffusion tensor imaging findings as biomarkers for amyotrophic lateral sclerosis. *Sci. Rep.* 10, 5199. doi: 10.1038/s41598-020-62049-0

Basser, P. J., Mattiello, J., and LeBihan, D. (1994). MR diffusion tensor spectroscopy and imaging. *Biophys. J.* 66, 259–267. doi: 10.1016/S0006-3495(94)80775-1

Baxi, M., Di Biase, M. A., Lyall, A. E., Cetin-Karayumak, S., Seitz, J., Ning, L., et al. (2020). Quantifying genetic and environmental influence on gray matter microstructure using diffusion MRI. *Cereb. Cortex* 30, 6191–6205. doi: 10.1093/cercor/bhaa174

Bock, A. S., Olavarria, J. F., Leigland, L. A., Taber, E. N., Jespersen, S. N., Kroenke, C. D., et al. (2010). Diffusion tensor imaging detects early cerebral cortex abnormalities in neuronal architecture induced by bilateral neonatal enucleation: an experimental model in the ferret. *Front. Syst. Neurosci.* 4, 149. doi: 10.3389/fnsys.2010.00149

Boscolo Galazzo, I., Brusini, L., Obertino, S., Zucchelli, M., Granziera, C., Menegaz, G., et al. (2018). On the Viability of diffusion MRI-based microstructural biomarkers in ischemic stroke. *Front. Neurosci.* 12, 92. doi: 10.3389/fnins.2018.00092

Brodmann, K. (1909). *Vergleichende Lokalisationslehre der Grosshirnrinde in ihren Prinzipien dargestellt auf Grund des Zellenbaues*. Leipzig: Barth.

Casanova, M. F., Buxhoeveden, D. P., Switala, A. E., and Roy, E. (2002). Neuronal density and architecture (Gray Level Index) in the brains of autistic patients. *J. Child. Neurol.* 17, 515–521. doi: 10.1177/088307380201700708

- Cho, Y. T., Fudge, J. L., and Ross, D. A. (2016). The architecture of cortex—in illness and in health. *Biol. Psychiatry*, 80, e95–e97. doi: 10.1016/j.biopsych.2016.10.010
- Coloigner, J., Batail, J.-M., Commowick, O., Corouge, I., Robert, G., Barillot, C., et al. (2019). White matter abnormalities in depression: a categorical and phenotypic diffusion MRI study. *Neuroimage. Clin.* 22, 101710. doi: 10.1016/j.nicl.2019.101710
- Cusick, C. G., Wall, J. T., Felleman, D. J., and Kaas, J. H. (1989). Somatotopic organization of the lateral sulcus of owl monkeys: area 3b, S-II, and a ventral somatosensory area. *J. Comp. Neurol.* 282, 169–190. doi: 10.1002/cne.902820203
- d'Alessandro, J., Barbier-Chebbah, A., Cellerin, V., Benichou, O., Mège, R. M., Voituriez, R., et al. (2021). Cell migration guided by long-lived spatial memory. *Nat. Commun.* 12, 4118. doi: 10.1038/s41467-021-24249-8
- de Góis Morais, P. L., de Lima, R. R., Ríos-Flórez, J. A., Melo, T. F., Clascá, F., de Souza Cavalcante, J., et al. (2020). Cytoarchitecture and myeloarchitecture of the entorhinal cortex of the common marmoset monkey (*Callithrix jacchus*). *J. Comp. Neurol.* 528, 1307–1320. doi: 10.1002/cne.24814
- Dubach, M. and Bowden, D. (2009). *BrainInfo Online 3d Macaque Brain Atlas: A Database of the Shape of a Brain*. Society for Neuroscience Annual Meeting, Chicago, IL Abstract No. 199, 5.
- Dyrby, T. B., Innocenti, G. M., Bech, M., and Lundell, H. (2018). Validation strategies for the interpretation of microstructure imaging using diffusion MRI. *Neuroimage* 182, 62–79. doi: 10.1016/j.neuroimage.2018.06.049
- Eickhoff, S. B., Grefkes, C., Zilles, K., and Fink, G. R. (2007). The somatotopic organization of cytoarchitectonic areas on the human parietal operculum. *Cereb. Cortex* 17, 1800–1811. doi: 10.1093/cercor/bhl090
- Elman, J. A., Panizzon, M. S., Hagler, D. J., Fennema-Notestine, C., Eyler, L. T., Gillespie, N. A., et al. (2017). Genetic and environmental influences on cortical mean diffusivity. *Neuroimage* 146, 90–99. doi: 10.1016/j.neuroimage.2016.11.032
- Estrada, L. I., Robinson, A. A., Amaral, A. C., Giannaris, E. L., Heyworth, N. C., Mortazavi, F., et al. (2017). Evaluation of long-term cryostorage of brain tissue sections for quantitative histochemistry. *J. Histochem Cytochem.* (2017) 65:153–171. doi: 10.1369/0022155416686934
- Fedorov, A., Beichel, R., Kalpathy-Cramer, J., Finet, J., Fillion-Robin, J. C., Pujol, S., et al. (2012). 3D Slicer as an image computing platform for the Quantitative Imaging Network. *Magn. Reson. Imaging*, 30, 1323–1341. doi: 10.1016/j.mri.2012.05.001
- Fink, G. R., Frackowiak, R. S., Pietrzyk, U., and Passingham, R. E. (1997). Multiple nonprimary motor areas in the human cortex. *J. Neurophysiol.* 77, 2164–2174. doi: 10.1152/jn.1997.77.4.2164
- Gao, Y., Choe, A. S., Stepniewska, I., Li, X., Avison, M. J., Anderson, A. W., et al. (2013). Validation of DTI tractography-based measures of primary motor area connectivity in the squirrel monkey brain. *PLoS ONE* 8, e75065. doi: 10.1371/journal.pone.0075065
- Giguère, N., Burke Nanni, S., and Trudeau, L.-E. (2018). On cell loss and selective vulnerability of neuronal populations in Parkinson's disease. *Front. Neurol.* 9, 455. doi: 10.3389/fneur.2018.00455
- Giorgio, A., Santelli, L., Tomassini, V., Bosnell, R., Smith, S., and Stefano, D., et al. (2010). Age-related changes in grey and white matter structure throughout adulthood. *Neuroimage* 51, 943–951. doi: 10.1016/j.neuroimage.2010.03.004
- Goldman-Rakic, P. S. (1982). Cytoarchitectonic heterogeneity of the primate neostriatum: subdivision into island and matrix cellular compartments. *J. Comp. Neurol.* 205, 398–413. doi: 10.1002/cne.902050408
- Götz, M., Nakafuku, M., and Petrik, D. (2016). Neurogenesis in the developing and adult brain—similarities and key differences. *Cold. Spring. Harb. Perspect. Biol.* 8, a018853. doi: 10.1101/cshperspect.a018853
- Gustavson, D. E., Hatton, S. N., Elman, J. A., Panizzon, M. S., Franz, C. E., Hagler, D. J., et al. (2019). Predominantly global genetic influences on individual white matter tract microstructure. *Neuroimage* 184, 871–880. doi: 10.1016/j.neuroimage.2018.10.016
- Gutierrez, C. E., Skibbe, H., Nakae, K., Tsukada, H., Lienard, J., Watakabe, A., et al. (2020). Optimization and validation of diffusion MRI-based fiber tracking with neural tracer data as a reference. *Sci. Rep.* 10, 21285. doi: 10.1038/s41598-020-78284-4
- Harrison, P. J., Colbourne, L., and Harrison, C. H. (2020). The neuropathology of bipolar disorder: systematic review and meta-analysis. *Mol. Psychiatry* 25, 1787–1808. doi: 10.1038/s41380-018-0213-3
- Hosseinbor, A. P., Chung, M. K., Wu, Y.-C., and Alexander, A. L. (2013). Bessel Fourier orientation reconstruction (BFOR): an analytical diffusion propagator reconstruction for hybrid diffusion imaging and computation of q-space indices. *Neuroimage* 64, 650–670. doi: 10.1016/j.neuroimage.2012.08.072
- Huttenlocher, P. R. (1979). Synaptic density in human frontal cortex - developmental changes and effects of aging. *Brain Res.* 163, 195–205. doi: 10.1016/0006-8993(79)90349-4
- Huttenlocher, P. R. (1984). Synapse elimination and plasticity in developing human cerebral cortex. *Am. J. Ment. Defic.* 88, 488–496.
- Ianuș, A., Carvalho, J., Fernandes, F. F., Cruz, R., Chavarrias, C., Palombo, M., et al. (2021). Soma and neurite density MRI (SANDI) of the in-vivo mouse brain. *bioRxiv* 08, 455923. doi: 10.1101/2021.08.11.455923
- Inglese, M. and Bester, M. (2010). Diffusion imaging in multiple sclerosis: research and clinical implications. *NMR Biomed.* 23, 865–872. doi: 10.1002/nbm.1515
- Jespersen, S. N., Leigland, L. A., Cornea, A., and Kroenke, C. D. (2012). Determination of axonal and dendritic orientation distributions within the developing cerebral cortex by diffusion tensor imaging. *IEEE Trans. Med. Imaging* 31, 16–32. doi: 10.1109/TMI.2011.2162099
- Jones, D. K. and Cercignani, M. (2010). Twenty-five pitfalls in the analysis of diffusion MRI data. *NMR Biomed.* 23, 803–820. doi: 10.1002/nbm.1543
- Khan, A. R., Chuhutin, A., Wiborg, O., Kroenke, C. D., Nyengaard, J. R., Hansen, B., et al. (2016). Biophysical modeling of high field diffusion MRI demonstrates micro-structural aberration in chronic mild stress rat brain. *Neuroimage* 142, 421–430. doi: 10.1016/j.neuroimage.2016.07.001
- Khaw, Y. M., Tierney, A., Cunningham, C., Soto-Díaz, K., Kang, E., Steelman, A. J., et al. (2021). Astrocytes lure CXCR2-expressing CD4+ T cells to gray matter via TAK1-mediated chemokine production in a mouse model of multiple sclerosis. *PNAS* 118, e2017213118. doi: 10.1073/pnas.2017213118
- Kikinis, Z., Makris, N., Sydnor, V. J., Bouix, S., Pasternak, O., Coman, I. L., et al. (2019). Abnormalities in gray matter microstructure in young adults with 22q11.2 deletion syndrome. *NeuroImage: Clin.* 21, 101611. doi: 10.1016/j.nicl.2018.10.1611
- Kroenke, C. D., Van Essen, D. C., Inder, T. E., Rees, S., Brethorst, G. L., Neil, J. J., et al. (2007). Microstructural changes of the baboon cerebral cortex during gestational development reflected in magnetic resonance imaging diffusion anisotropy. *J. Neurosci.* 27, 12506–12515. doi: 10.1523/JNEUROSCI.3063-07.2007
- Krubitzer, L. A. and Kaas, J. H. (1990). The organization and connections of somatosensory cortex in marmosets. *J. Neurosci.* 10, 952–974. doi: 10.1523/JNEUROSCI.10-03-00952.1990
- Kubicki, M., Baxi, M., Pasternak, O., Tang, Y., Karmacharya, S., Chunga, N., et al. (2019). Lifespan trajectories of white matter changes in rhesus monkeys. *Cereb. Cortex* 29, 1584–1593. doi: 10.1093/cercor/bhy056
- Kubicki, M., McCarley, R., Westin, C. F., Park, H. J., Maier, S., Kikinis, R., et al. (2007). A review of diffusion tensor imaging studies in schizophrenia. *J. Psychiatr. Res.* 41, 15–30. doi: 10.1016/j.jpsychires.2005.05.005
- Laitinen, T., Sierra, A., Bolkvadze, T., Pitkänen, A., and Gröhn, O. (2015). Diffusion tensor imaging detects chronic microstructural changes in white and gray matter after traumatic brain injury in rat. *Front. Neurosci.* 9, 128. doi: 10.3389/fnins.2015.00128
- Le, H., Zeng, W., Zhang, H., Li, J., Wu, X., Xie, M., et al. (2020). Mean apparent propagator MRI is better than conventional diffusion tensor imaging for the evaluation of Parkinson's disease: a prospective pilot study. *Front. Aging Neurosci.* 12, 306. doi: 10.3389/fnagi.2020.563595
- Lebel, C., Gee, M., Camicioli, R., Wieler, M., Martin, W., Beaulieu, C., et al. (2012). Diffusion tensor imaging of white matter tract evolution over the lifespan. *Neuroimage* 60, 340–352. doi: 10.1016/j.neuroimage.2011.11.094
- Leergaard, T. B., White, N. S., De Crespigny, A., Bolstad, I., D'Arceuil, H., Bjaalie, J. G., et al. (2010). Quantitative histological validation of diffusion MRI fiber orientation distributions in the rat brain. *PLoS ONE* 5, e8595. doi: 10.1371/journal.pone.0008595
- Lerch, J. P., Gazdzinski, L., Germann, J., Sled, J. G., Henkelman, R. M., Nieman, B. J., et al. (2012). Wanted dead or alive? The tradeoff between in-vivo versus ex-vivo MR brain imaging in the mouse. *Front. Neuroinform.* 6, 6. doi: 10.3389/fninf.2012.00006
- Leuze, C., Goubran, M., Barakovic, M., Aswendt, M., Tian, Q., Hsueh, B., et al. (2021). Comparison of diffusion MRI and CLARITY fiber orientation estimates in both gray and white matter regions of human and primate brain. *NeuroImage* 228, 117692. doi: 10.1016/j.neuroimage.2020.117692
- Maiter, A., Riemer, F., Allinson, K., Zaccagna, F., Crispin-Ortuzar, M., Gehrung, M., et al. (2021). Investigating the relationship between diffusion kurtosis tensor imaging (DKTI) and histology within the normal human brain. *Sci. Rep.* 11, 8857. doi: 10.1038/s41598-021-87857-w
- Martínez-Pinilla, E., Ordóñez, C., del Valle, E., Navarro, A., and Tolivia, J. (2016). Regional and gender study of neuronal density in brain during aging and in Alzheimer's disease. *Front. Aging Neurosci.* 8, 213. doi: 10.3389/fnagi.2016.00213

- Mulkern, R. V., Gudbjartsson, H., Westin, C. F., Zengingonul, H. P., Gartner, W., Guttman, C. R., et al. (1999). Multi-component apparent diffusion coefficients in human brain. *NMR Biomed.* 12, 51–62.
- Muraki, K. and Tanigaki, K. (2015). Neuronal migration abnormalities and its possible implications for schizophrenia. *Front. Neurosci.* 9, 74. doi: 10.3389/fnins.2015.00074
- Nakafuku, M. and Del Águila, Á. (2020). Developmental dynamics of neurogenesis and gliogenesis in the postnatal mammalian brain in health and disease: historical and future perspectives. *Wiley Interdiscip. Rev. Dev. Biol.* 9, e369. doi: 10.1002/wdev.369
- Ning, L., Westin, C.-F., and Rathi, Y. (2015). Estimating diffusion propagator and its moments using directional radial basis functions. *IEEE Trans. Med. Imaging* 34, 2058–2078. doi: 10.1109/TMI.2015.2418674
- O'Donnell, L. J. and Westin, C.-F. (2011). An introduction to diffusion tensor image analysis. *Neurosurv. Clin.* 22, 185–196. doi: 10.1016/j.nec.2010.12.004
- Özarslan, E., Koay, C. G., Shepherd, T. M., Komlosh, M. E., Irfanoglu, M. O., Pierpaoli, C., et al. (2013). Mean apparent propagator (MAP) MRI: a novel diffusion imaging method for mapping tissue microstructure. *Neuroimage* 78, 16–32. doi: 10.1016/j.neuroimage.2013.04.016
- Palombo, M., Ianus, A., Guerrerri, M., Nunes, D., Alexander, D. C., Shemesh, N., et al. (2020). SANDI: a compartment-based model for non-invasive apparent soma and neurite imaging by diffusion MRI. *Neuroimage* 215, 116835. doi: 10.1016/j.neuroimage.2020.116835
- Rakic, P., Bourgeois, J. P., Eckenhoff, M. F., Zecevic, N., and Goldman-Rakic, P. S. (1986). Concurrent overproduction of synapses in diverse regions of the primate cerebral cortex. *Science* 232, 232–235. doi: 10.1126/science.3952506
- Rane, S. and Duong, T. Q. (2011). Comparison of in vivo and ex vivo diffusion tensor imaging in rhesus macaques at short and long diffusion times. *Open Neuroimag. J.* 5, 172–178. doi: 10.2174/187444001105010172
- Rathi, Y., Gagoski, B., Setsompop, K., Michailovich, O., Grant, P. E., Westin, C., et al. (2013). Diffusion propagator estimation from sparse measurements in a tractography framework. *Med. Image Comput. Comput. Assist. Interv.* 16, 510–517. doi: 10.1007/978-3-642-40760-4_64
- Rathi, Y., Pasternak, O., Savadjiev, P., Michailovich, O., Bouix, S., Kubicki, M., et al. (2014). Gray matter alterations in early aging: a diffusion magnetic resonance imaging study. *Hum. Brain Mapp.* 35, 3841–3856. doi: 10.1002/hbm.22441
- Roebroek, A., Miller, K. L., and Aggarwal, M. (2019). Ex vivo diffusion MRI of the human brain: technical challenges and recent advances. *NMR Biomed.* 32, e3941. doi: 10.1002/nbm.3941
- Rohlfing, T., Kroenke, C., Sullivan, E., Dubach, M., Bowden, D., Grant, K., et al. (2012). The INIA19 template and neuromaps atlas for primate brain image parcellation and spatial normalization. *Front. Neuroinform.* 6, 27. doi: 10.3389/fninf.2012.00027
- Rosene, D. L., Roy, N. J., and Davis, B. J. (1986). A cryoprotection method that facilitates cutting frozen sections of whole monkey brains for histological and histochemical processing without freezing artifact. *J. Histochem. Cytochem.* 34, 1301–1315. doi: 10.1177/34.10.3745909
- Salo, R. A., Belevich, I., Jokitalo, E., Gröhn, O., and Sierra, A. (2021). Assessment of the structural complexity of diffusion MRI voxels using 3D electron microscopy in the rat brain. *NeuroImage* 225, 117529. doi: 10.1016/j.neuroimage.2020.117529
- Saunders, R. C., Aigner, T. G., and Frank, J. A. (1990). Magnetic resonance imaging of the rhesus monkey brain: use for stereotactic neurosurgery. *Exp. Brain Res.* 81, 443–446. doi: 10.1007/BF00228139
- Schilling, K. G., Janve, V., Gao, Y., Stepniewska, L., Landman, B. A., Anderson, A. W., et al. (2018). Histological validation of diffusion MRI fiber orientation distributions and dispersion. *Neuroimage* 165, 200–221. doi: 10.1016/j.neuroimage.2017.10.046
- Seehaus, A., Roebroek, A., Bastiani, M., Fonseca, L., Bratzke, H., Lori, N., et al. (2015). Histological validation of high-resolution DTI in human post mortem tissue. *Front. Neuroanat.* 9, 98. doi: 10.3389/fnana.2015.00098
- Seitz, J., Rathi, Y., Lyall, A., Pasternak, O., Del Re, E. C., Niznikiewicz, M., et al. (2018). Alteration of gray matter microstructure in schizophrenia. *Brain Imaging Behav.* 12, 54–63. doi: 10.1007/s11682-016-9666-7
- Semendeferi, K., Armstrong, E., Schleicher, A., Zilles, K., and Van Hoesen, G. W. (2001). Prefrontal cortex in humans and apes: A comparative study of area 10. *Am. J. Phys. Anthropol.* 114, 224–241. Available online at: doi: 10.1002/1096-8644(200103)114:3<224::AID-AJPA1022>3.0.CO;2-I
- Sewards, T. V. and Sewards, M. A. (2003). Input and output stations of the entorhinal cortex: superficial vs. deep layers or lateral vs. medial divisions? *Brain Res. Rev.* 42, 243–251. doi: 10.1016/S0165-0173(03)00175-9
- Shimony, J. S., Rutlin, J., Karimi, M., Tian, L., Snyder, A. Z., Loftin, S. K., et al. (2018). Validation of diffusion tensor imaging measures of nigrostriatal neurons in macaques. *PLoS ONE* 13, e0202201. doi: 10.1371/journal.pone.0202201
- Siegel, R. J., Swan, K., Edwalds, G., and Fishbein, M. C. (1985). Limitations of postmortem assessment of human coronary artery size and luminal narrowing: differential effects of tissue fixation and processing on vessels with different degrees of atherosclerosis. *J. Am. Coll. Cardiol.* 5, 342–346. doi: 10.1016/S0735-1097(85)80056-5
- Sikora, E., Bielak-Zmijewska, A., Dudkowska, M., Krzystyniak, A., Mosieniak, G., Wesierska, M., et al. (2021). Cellular senescence in brain aging. *Front. Aging Neurosci.* 13, 71. doi: 10.3389/fnagi.2021.646924
- Smith, S. M. (2002). Fast robust automated brain extraction. *Hum. Brain Mapp.* 17, 143–155. doi: 10.1002/hbm.10062
- Smith, S. M., Jenkinson, M., Woolrich, M. W., Beckmann, C. F., Behrens, T. E. J., Johansen-Berg, H., et al. (2004). Advances in functional and structural MR image analysis and implementation as FSL. *NeuroImage, Mathematics in Brain Imaging* 23, S208–S219. doi: 10.1016/j.neuroimage.2004.07.051
- Stebbins, G. T. and Murphy, C. M. (2009). Diffusion tensor imaging in Alzheimer's disease and mild cognitive impairment. *Behav. Neurol.* 21, 39–49. doi: 10.1155/2009/915041
- Stockmeier, C. A. and Rajkowska, G. (2004). Cellular abnormalities in depression: evidence from postmortem brain tissue. *Dialogues Clin. Neurosci.* 6, 185–197. doi: 10.31887/DCNS.2004.6.2/cstockmeier
- Tanner, C. M., Ottman, R., Goldman, S. M., Ellenberg, J., Chan, P., Mayeux, R., et al. (1999). Parkinson disease in twins: an etiologic study. *JAMA* 281, 341–346. doi: 10.1001/jama.281.4.341
- Tee, J. Y., Sutharsan, R., Fan, Y., and Mackay-Sim, A. (2017). Cell migration in schizophrenia: patient-derived cells do not regulate motility in response to extracellular matrix. *Mol. Cell. Neurosci.* 80, 111–122. doi: 10.1016/j.mcn.2017.03.005
- Tigges, J., Gordon, T. P., McClure, H. M., Hall, E. C., and Peters, A. (1988). Survival rate and life span of rhesus monkeys at the Yerkes regional primate research center. *Am. J. Primatol.* 15, 263–273. doi: 10.1002/ajp.1350150308
- Veraart, J., Novikov, D. S., Christiaens, D., Ades-aron, B., Sijbers, J., and Fieremans, E. (2016). Denoising of diffusion MRI using random matrix theory. *Neuroimage* 142, 394–406. doi: 10.1016/j.neuroimage.2016.08.016
- Vogt, C. and Vogt, O. (1926). Die vergleichend-architektonische und die vergleichend-reizphysiologische Felderung der Großhirnrinde unter besonderer Berücksichtigung der menschlichen. *Naturwissenschaften* 14, 1190–1194. doi: 10.1007/BF01451766
- Vuoksima, E., Panizzon, M. S., Hagler Jr, D. J., Hatton, S. N., Fennema-Notestine, C., Rinker, D., et al. (2017). Heritability of white matter microstructure in late middle age: a twin study of tract-based fractional anisotropy and absolute diffusivity indices. *Hum. Brain Mapp.* 38, 2026–2036. doi: 10.1002/hbm.23502
- Williams, M. R., Marsh, R., Macdonald, C. D., Jain, J., Pearce, R. K. B., Hirsch, S. R., et al. (2013). Neuropathological changes in the nucleus basalis in schizophrenia. *Eur. Arch. Psychiatry Clin. Neurosci.* 263, 485–495. doi: 10.1007/s00406-012-0387-7
- Wu, W., McNulty, G., Hamoda, H. M., Sarill, K., Karmacharya, S., Gagoski, B., et al. (2019). Detecting microstructural white matter abnormalities of frontal pathways in children with ADHD using advanced diffusion models. *Brain Imaging Behav.* 14:981–997. doi: 10.1007/s11682-019-00108-5
- Wu, Y.-C. and Alexander, A. L. (2007). Hybrid diffusion imaging. *NeuroImage* 36, 617–629. doi: 10.1016/j.neuroimage.2007.02.050
- Yendiki, A., Aggarwal, M., Axer, M., Howard, A. F. D., van Cappellen van Walsum, A.-M., and Haber, S. N. (2021). Post mortem mapping of connective anatomy for the validation of diffusion MRI. *bioRxiv* 04, 440223. doi: 10.1101/2021.04.16.440223
- Yoshida, S., Oishi, K., Faria, A. V., and Mori, S. (2013). Diffusion tensor imaging of normal brain development. *Pediatr. Radiol.* 43, 15–27. doi: 10.1007/s00247-012-2496-x
- Zatorre, R. J., Fields, R. D., and Johansen-Berg, H. (2012). Plasticity in gray and white: neuroimaging changes in brain structure during learning. *Nat. Neurosci.* 15, 528–536. doi: 10.1038/nn.3045
- Zhang, J., Wei, R. L., Peng, G. P., Zhou, J. J., Wu, M., He, F. P., et al. (2017). Correlations between diffusion tensor imaging and levels of consciousness in patients with traumatic brain injury: a systematic review and meta-analysis. *Sci. Rep.* 7, 2793. doi: 10.1038/s41598-017-02950-3
- Zhang, Y. and Burock, M. A. (2020). Diffusion tensor imaging in Parkinson's disease and Parkinsonian syndrome: a systematic review. *Front. Neurol.* 11, 1091. doi: 10.3389/fneur.2020.531993
- Zhou, Z., Tong, Q., Zhang, L., Ding, Q., Lu, H., Jonkman, L. E., et al. (2020). Evaluation of the diffusion MRI white matter tract integrity model using myelin histology and Monte-Carlo simulations. *NeuroImage* 223, 117313. doi: 10.1016/j.neuroimage.2020.117313